

## Raman and Photoluminescence Properties of Type II GaSb/GaAs Quantum Dots on (001) Ge Substrate

Zon,<sup>1</sup> Thanavorn Poempool,<sup>1</sup> Suwit Kiravittaya,<sup>2</sup> Noppadon Nuntawong,<sup>3</sup> Suwat Sopitpan,<sup>4</sup> Supachok Thainoi,<sup>1</sup> Songphol Kanjanachuchai,<sup>1</sup> Somchai Ratanathammaphan,<sup>1</sup> and Somsak Panyakeow<sup>1,\*</sup>

<sup>1</sup>Semiconductor Device Research Laboratory (SDRL), Department of Electrical Engineering,  
Faculty of Engineering, Chulalongkorn University, Bangkok 10330, Thailand

<sup>2</sup>Advanced Optical Technology Laboratory, Department of Electrical and Computer Engineering,  
Faculty of Engineering, Naresuan University, Phitsanulok 65000, Thailand

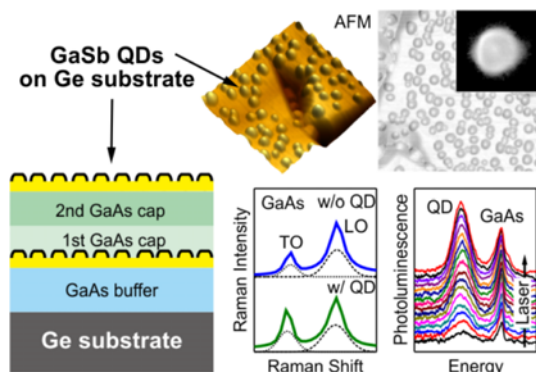
<sup>3</sup>National Electronics and Computer Technology Center (NECTEC), National Science and Technology  
Development Agency (NSTDA), Pathumthani 12120, Thailand

<sup>4</sup>Thailand Microelectronics Center (TMEC), National Science and Technology Development Agency (NSTDA),  
Chachoengsao 24000, Thailand

(received date: 4 January 2016 / accepted date: 26 April 2016 / published date: 10 July 2016)

We investigate structural Raman and photoluminescence properties of type II GaSb/GaAs quantum dots (QDs) grown on (001) Ge substrate by molecular beam epitaxy. Array of self-assembled GaSb QDs having an areal density of  $\sim 1.66 \times 10^{10}$  dots/cm<sup>2</sup> is obtained by a growth at relatively low substrate temperature (450 °C) on a GaAs surface segmented into anti-phase domains (APDs). Most of QDs form in one APD area. However, a few QDs can be observed at the APD boundaries. Raman spectroscopy is used to probe the strain in GaAs layer. Slight redshift of both LO and TO GaAs peaks are observed when GaSb QDs are buried into GaAs matrix. Optical properties of capped QDs are characterized by photoluminescence measurement at low temperatures (20 K and 30 K). Emission peaks of GaSb/GaAs QDs are found in the range of 1.0-1.3 eV at both temperatures. Slight redshift is observed when the laser excitation power is increased at 20 K while blueshift of QD peak is observed at 30 K. We attribute this abnormal behavior to the contribution of overlapped GaSb wetting layer peak in the PL emission as well as the feature of type II band structure.

**Keywords:** GaSb, quantum dot, Ge substrate, photoluminescence



### 1. INTRODUCTION

In recent years, semiconductor quantum dots (QDs) based on III-V compounds have attracted much attention as the next generation nanostructures for novel devices such as intermediate band solar cell.<sup>[1]</sup> Combinational concept of III-

V nanostructured solar cell is our research interests.<sup>[2,3]</sup> Most of studied III-V QD material systems has type I band alignment e.g. InAs/GaAs. The nature of this system is that both electrons and holes are confined in QD, and results in fast recombination rate, which is an unfavorable property of absorbing layer in an intermediate band solar cell.<sup>[1]</sup> On the contrary, type II QD has only one type of carriers confined in QD. Less overlapping between electron and hole wave functions results in a long carrier lifetime, which is a desired

\*Corresponding author: somsak.p@chula.ac.th  
©KIM and Springer

property for photovoltaic applications.<sup>[1,4,5]</sup>

Our approach to develop the nanostructured solar cell is to combine with the usage of Ge substrate.<sup>[6,7]</sup> Nearly lattice matched condition (between Ge and GaAs) allows one to fabricate high efficiency solar cells for space applications.<sup>[8]</sup> Natural formation of anti-phase domains (APDs) across the GaAs layer on Ge due to opposite domains polarity<sup>[6,9]</sup> makes us concentrate on the epitaxial step. In our former study, we have shown that GaSb/GaAs QDs can be grown on (001) Ge substrate.<sup>[7]</sup> The lattice mismatch ( $\sim 7.8\%$ ) between GaSb and GaAs interface is similar to the type I InAs/GaAs heterostructure. The large band offset between GaSb QDs and GaAs matrix ( $\sim 0.7$  eV) induces strong hole localization in QDs.<sup>[4,5,10,11]</sup> Therefore, type II GaSb/GaAs system deserves for not only photovoltaic applications but also detecting devices such as infrared detectors and memory devices.<sup>[10]</sup>

In this work, we have investigated the growth and optical properties of GaSb/GaAs QDs grown on (001) Ge substrate. The structural and optical properties of GaSb/GaAs QDs are characterized by atomic force microscopy (AFM) and low-temperatures (20 K and 30 K) power-dependent photoluminescence (PL) measurement. The strain induced effect corresponds to the present of QD layer is analyzed by Raman spectroscopy.

## 2. EXPERIMENTAL PROCEDURE

The sample is fabricated by using a molecular beam epitaxy (MBE) machine (RIBER, Compact 21TM) equipped with antimony (Sb) valved cracker cell. Due to the large lattice mismatch between GaSb and GaAs, self-assembled QDs can be formed in Stranski-Krastanov mode. Figure 1 shows the schematic of our sample structure for investigating both structural and optical properties.

Experimental details are as follows. The surface oxide desorption of (001) Ge substrate is done at  $\sim 500$  °C under As<sub>4</sub>.<sup>[12]</sup> The growth starts by depositing 500-nm GaAs buffer layer at the deoxidation temperature. During the growth, reflection high-energy electron diffraction (RHEED) pattern

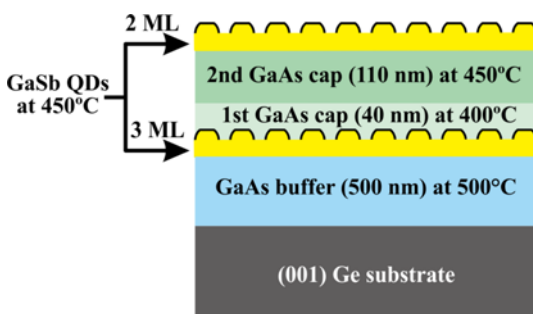


**Fig. 1.** Schematic sample structure of type II GaSb/GaAs QDs on (001) Ge substrate.

is always observed. The (2  $\times$  2)-to-c(4  $\times$  4) RHEED pattern transition is used to calibrate the surface temperature.<sup>[13]</sup> For the buffer layer growth, the V/III flux ratio is kept at  $\sim 13$ . The GaAs growth rate is 0.51 monolayer/s (ML/s). After the buffer layer growth, arsenic cell temperature is cooled down in order to have an arsenic-free atmosphere for GaSb QD growth. The substrate temperature is also ramped down to 450 °C. GaSb/GaAs QDs are grown at the V/III ratio of  $\sim 4$  with the growth rate of 0.14 ML/s. Note that 60-s Sb soaking is performed before opening Ga shutter. The GaSb QD growth is stopped at  $\sim 3$ -ML GaSb deposition (22 sec). For preserving QDs after the growth, the substrate temperature is reduced to 400 °C. GaSb QDs are capped by 40-nm GaAs at this temperature. This growth step is performed in order to avoid dissolving of GaSb QDs during capping.<sup>[14]</sup> Then 110-nm GaAs layer is further grown at 450 °C. To investigate the surface morphology by AFM, 2 ML GaSb QDs are grown on the surface with the same conditions. The Ga cell shutter is opened for 15 s to perform 2 ML QDs growth.

After growth, the sample is characterized by AFM (Seiko SPA-400) in dynamic force mode in air. Slow scan speed (0.5 Hz) is used to improve the image quality. Raman spectroscopy is carried out by using room temperature (RT) Invia Reflex Confocal Raman spectrometer with 532-nm laser. The photoluminescence (PL) measurement is carried out at low temperatures (20 K and 30 K) by using 514.5-nm Ar<sup>+</sup> laser as an excitation laser source and cooled down InGaAs photodetector.

## 3. RESULTS AND DISCUSSION

### 3.1 Surface morphology of GaSb/GaAs quantum dots

Figure 2(a) shows a 3D AFM image of GaSb/GaAs QDs formed on (001) Ge substrate. Although the lattice mismatch between GaAs and Ge is a quite low ( $\sim 0.1\%$ ), the growth of polar (GaAs) on nonpolar (Ge) materials induces the APD formation. The crack-like surface structures due to the formation of APD with APD boundary (APB) can be clearly observed in the Fig. 2(a). Naturally, APDs are formed in two different orientations: As-As bond and Ga-Ga bond (90° rotated by each other) of GaAs deposited on Ge.<sup>[9,15]</sup> Normally, APBs act as non-radiative recombination centers. Therefore, growth parameters of GaAs buffer layer must be adjusted to suppress the formation of APBs (by enlarging the size of APDs). Apart from the APBs, one can also observe circular based GaSb/GaAs QDs in Fig. 2(b). Most QDs are formed in the flat area of each APD. Only a few QDs are also found along the APBs.

To investigate the QD at APB, we extract AFM line profiles through the QDs at an APB and in the APDs as shown in Figs. 2(c, d). The lines are drawn perpendicular to the investigated APB, which has a width of  $\sim 100$  nm. We found that the depth of the APB is not uniform (5-20 nm).

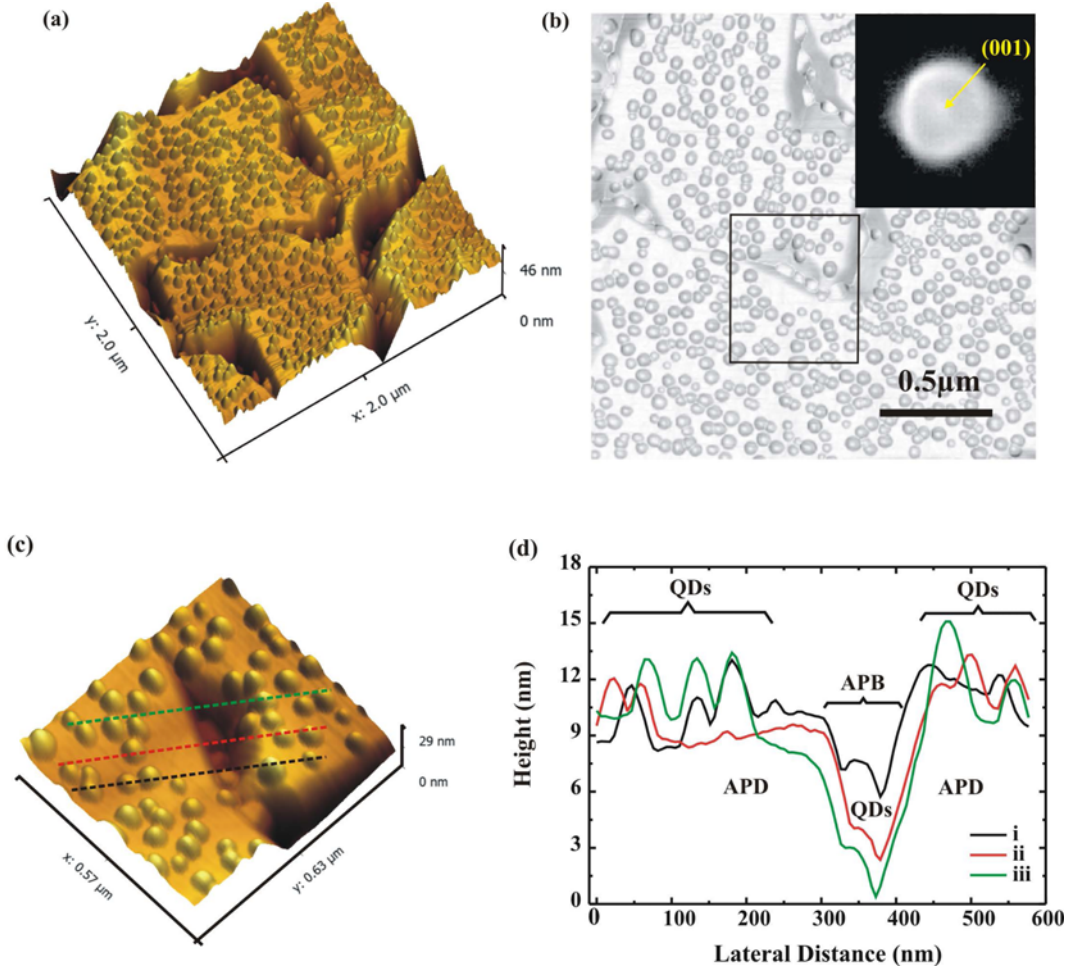


**Fig. 2.** (a)  $2 \times 2 \mu\text{m}^2$  3D AFM image with 2 ML GaSb QDs layer on (001) Ge substrate. (b)  $2 \times 2 \mu\text{m}^2$  2D AFM image in surface slope scale of (a). Upper right inset shows the facet plot of QD surface. The rectangle box marks an area of anti-phase domain boundaries (APB) and anti-phase domains (APDs) with the QDs. (c) 3D AFM image of the area in rectangle box of (b). (d) Line profiles of the QDs (i-iii) formed in both APB and APDs.

Three successive QDs on APD and APB are in serial (i-iii) from the shallowest QDs to the deepest one are shown in Figs. 2(c, d). All QDs at APBs tends to elongate along the APB direction.

Figures 3(a, b) show histograms of QD diameter in APDs and APBs and Figs. 3(c, d) show those of QD height in APDs and APBs. These data are extracted from AFM image of individual QD by taking the base line at the circular base shape of QD. Then the height and diameter data are fitted by Gaussian function. The GaSb/GaAs QDs in APDs have average dots diameters, heights and dots density of  $48.8 \pm 14.1 \text{ nm}$ ,  $4.47 \pm 1.27 \text{ nm}$  and  $\sim 1.57 \times 10^{10} \text{ cm}^{-2}$ , and that in APBs have  $82.1 \pm 13.6 \text{ nm}$ ,  $4.38 \pm 2.23 \text{ nm}$  and  $\sim 9.5 \times 10^8 \text{ cm}^{-2}$ , respectively. It can be seen that the diameter of size of QDs in APBs are larger than that in APDs. We speculate that both QDs (in APDs and APBs) give the same emission. Our former study<sup>[7]</sup> showed that similar QDs with higher areal density ( $1.9 \times 10^{10} \text{ cm}^{-2}$ ) could be obtained. By comparing

the AFM image of the former report and this result, we have seen that the size of APBs in this work is larger and therefore the flat GaAs area on each APD is reduced. Moreover, lower QD density might be due to slight difference of QD growth conditions.

### 3.2 Raman spectroscopy

Presence of GaSb QD layer (either free standing or buried ones) produces the strain influence to the neighboring GaAs layers. Raman scattering analysis is attempted to reveal the effects of strain from GaSb QD layer. Raman spectra obtained from samples without and with buried GaSb QDs are shown in Figs. 4(a) and (b). The peaks from optical phonon scattering of transverse optical phonon (TO) and longitudinal optical phonon (LO) modes of GaAs are mainly observed in these spectra. To quantify the peak position, Gaussian function fits are applied (See Fig. 4(b)). The fitted TO and LO peak positions at  $267.8 \text{ cm}^{-1}$  and  $290.6 \text{ cm}^{-1}$  are

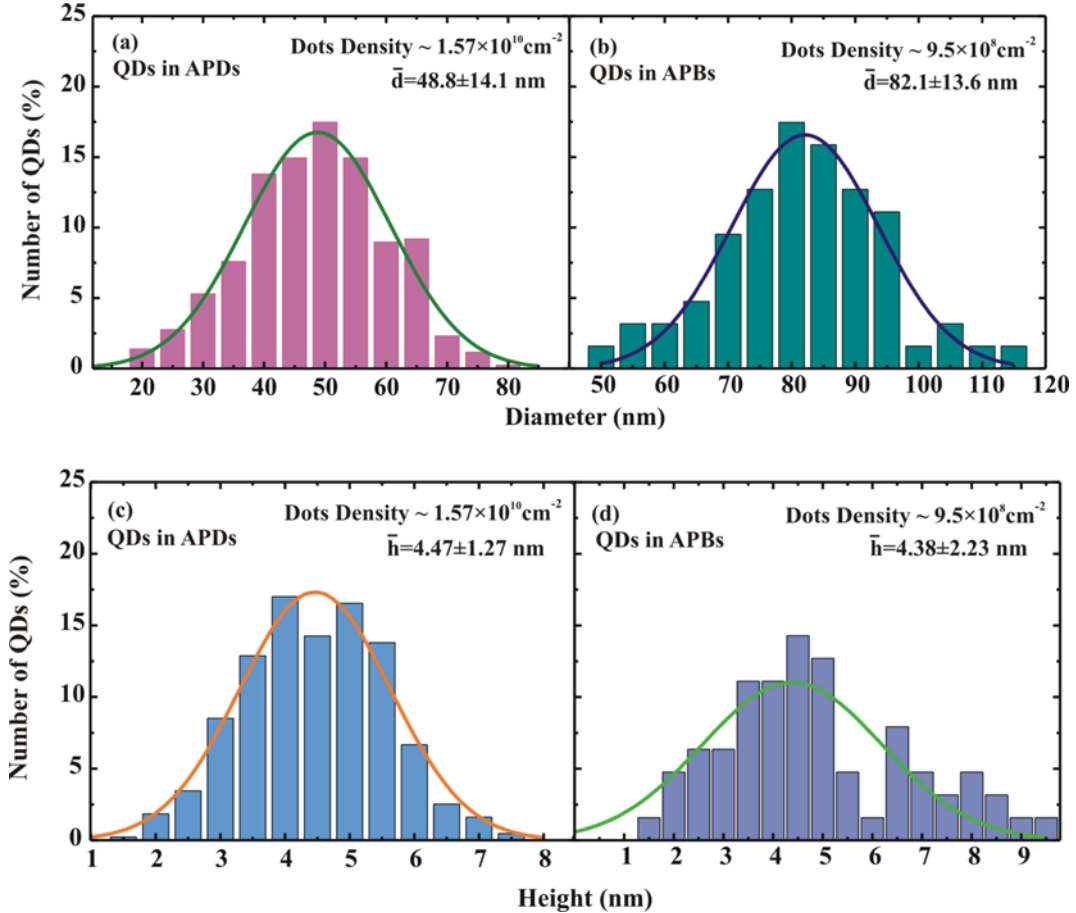


**Fig. 3.** (a-d) Histograms show the distributions of GaSb QDs by comparing diameters and height of QDs between APDs and along APBs. Solid lines are Gaussian fits. Dot density, mean and standard deviation of height and diameter values are shown.

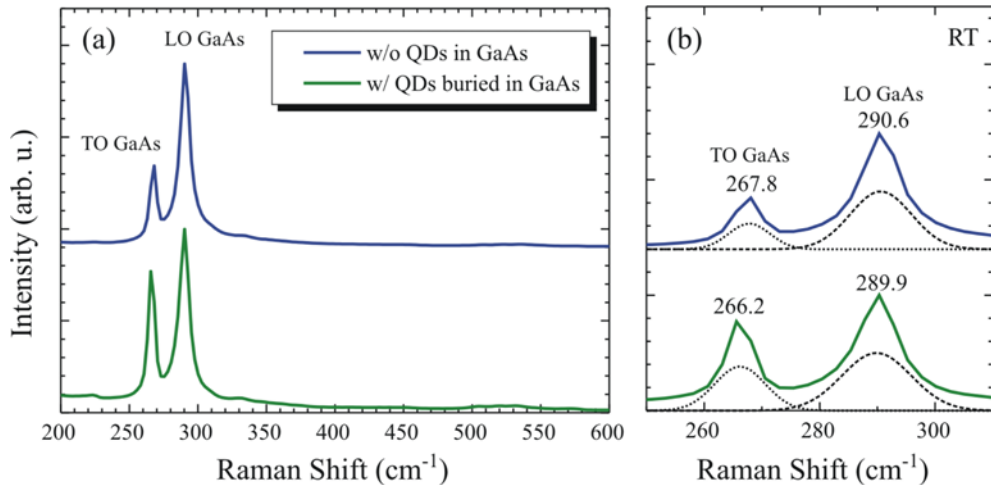


**Fig. 4.** (a) Normalized Raman spectra measured from the epitaxial GaAs samples without and with buried GaSb QDs and (b) Raman spectra described the redshift of TO and LO GaAs peaks due to the presence of GaSb QD layer. The dash and dotted lines are from Gaussian fits (shown with a division by one half).

detected in the spectrum obtained from the sample without buried GaSb QDs. With GaSb QDs, the TO and LO GaAs

peaks are shifted by  $1.6 \text{ cm}^{-1}$  and  $0.7 \text{ cm}^{-1}$  to  $266.2 \text{ cm}^{-1}$  and  $289.9 \text{ cm}^{-1}$ , respectively. These shifts are attributed to the

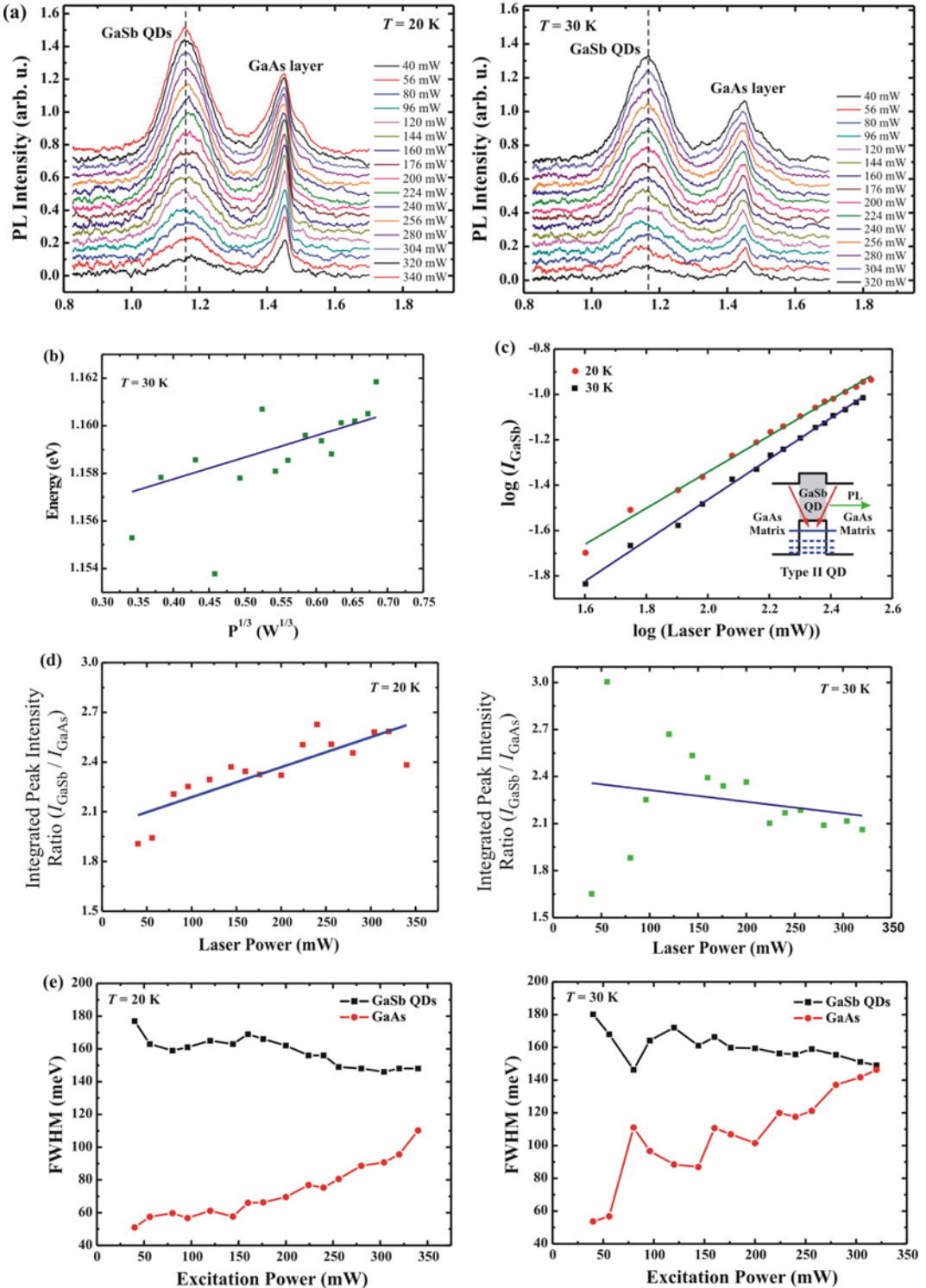


**Fig. 5.** (a) Power-dependent PL spectra at different temperatures (20 K and 30 K) obtained from GaSb/GaAs QDs on (001) Ge substrate. The vertical dash line marks the QD peak position of the spectrum at respective highest powers (340 mW/320 mW at 20 K/30 K). The higher power spectra are vertically offset for clarity. (b) The shift of the PL peaks energy as the third root of the excitation power at 30 K. Solid line is a linear fit. (c) The comparison of the integrated peak intensity of GaSb QDs versus laser excitation power in log-log scale between PL obtained at 20 K and 30 K. The inset is the band diagram demonstrating radiative recombination in type-II GaSb/GaAs QD. Solid line is a linear fit. (d) Ratio between integrated peak intensity of GaSb QDs and GaAs as a function of excitation power at respective different temperatures 20 K and 30 K. Solid line is a linear fit. (e) The comparison of full-width at half maximum (FWHM) between GaSb QDs and GaAs as a function of laser excitation power at 20 K and 30 K respectively.

introduction of tensile strain in GaAs matrix due to the presence of compressively strained GaSb QDs.<sup>[16]</sup>

### 3.3 Photoluminescence emission from GaSb/GaAs quantum dots

The PL spectroscopy of GaSb/GaAs QDs grown on (001) Ge substrate is performed to derive the optical properties of QDs. Power-dependent PL spectra at 20 K and 30 K are shown in Fig. 5(a). In the PL spectra, two distinct peaks can be seen. We attribute them to the emission from GaSb QDs (ranging between 1.0-1.3 eV) and GaAs layer (1.36 - 1.57 eV). The photo-response from GaSb QDs is at longer wavelength due to the lower bandgap energy. The intermixing of Sb/As at the interface between GaAs buffer layer and GaSb QDs/GaSb WL and that of As/Sb at the interface between GaSb QDs and GaAs cap layer are the reason of having QDs peak at very high energy as compared with GaSb bulk.<sup>[17,18]</sup> Moreover, we have not observed GaSb wetting layer (WL) peak, which is different from our former report.<sup>[7]</sup> The peaks energy position of WL can shift with respect to the thickness of deposited WL. The thicker the WL is, the lower the emission energy is.<sup>[19]</sup> We thus speculate that the WL is hidden in GaSb QD peak (1.0 - 1.3 eV). This results in a rather broad QD peak. In addition, combination of QD and WL peaks will give peculiar observation discussed below.

At 20 K, while the QD peak is quite broad, the GaAs peak shows a sharper and smoother peak. As the excitation power increased, the QD peak slightly shifts in both directions. However, the comparison between the result at minimum/maximum excitation powers (40/340 mW) shows that the QD peaks redshifted of about 12 meV. The redshift of the QD peak at higher excitation powers can be explained by the fact that at low excitation power, the main contribution to the QD peak is from the WL, which emits light at higher energy. When the excitation power increases, the QDs emit light more efficiently. By excluding two lower spectra, we found that QD PL peak energy is nearly constant at 1.16 eV. The GaSb QD peak intensity is higher than GaAs peak intensity at higher excitation power (224-340 mW). This indicates that the radiative recombination in GaSb QD is more efficient than that in bulk GaAs. When the temperature is increased to 30 K, the PL peaks slightly shift to higher energies as a function of excitation power, which is a feature of GaSb/GaAs type II band structure. It can be speculated that the peaks of GaSb QDs become dominant and that of WL becomes weak and convoluted in the broad QD peak at increased temperatures.<sup>[19]</sup> The blueshift of QD peak of about 6.6 meV is observed when the laser excitation power is changed from the lowest (40 mW) to the highest (320 mW) ones. In Fig. 5(b), it can be seen that the peak positions at low excitation powers shift slightly in both directions. This could be attributed to the participation of

WL peaks in the QD peaks, and it is not possible to extract the single QD peaks from the overlap peaks of QDs and WL. From our PL, the average hole localization energy, i.e., energy difference between QD and GaAs peaks, is 260 meV and 277 meV in the corresponding temperatures 20 K and 30 K. This large energy value might be useful for utilizing this QD as a cell in memory devices.<sup>[11]</sup>

By fitting each PL peak with Gaussian functions, quantitative data are obtained. In Figs. 5(c)-(e), the integrated peak intensity of GaSb QDs, the integrated peak intensity ratio of GaSb QDs to GaAs layer and the full width at half maximum (FWHM) are shown as a function of laser excitation powers (40-340 mW) at 20 K and (40-320 mW) at 30 K.

The relation between QD integrated peak intensity and excitation power at different temperatures are plotted in Fig. 5(c) to discuss about the transfer rate of holes from WL and GaAs cap layer to GaSb QDs. According to the graphs, the integrated peak intensity  $I_{\text{Gasb}}$  of QDs linearly increases with the increasing of excitation powers in both temperatures. This means that the steady exciton recombination occurs. At low laser power, the graph shows no good agreement with the linear fit due to the noise signal. At high excitation power value, the intensity starts to saturate. This early saturation of the integrated PL peak intensity is due to the slow recombination nature of carriers with time and the reduction of time-dependent band-bending effect in type II QD.

Figure 5(d) shows the ratio between integrated peak intensity of GaSb QD and GaAs at different temperatures. It increases when excitation power is increased at 20 K while it decreases when the excitation power is increased higher than 120 mW at 30 K. This result indicates that the radiative recombination in GaSb QD is still more efficient than that in bulk GaAs with APB at 20 K and that is getting less efficient at 30 K.

The comparison of FWHM between GaSb QDs and GaAs layer at different temperatures are shown in Fig. 5(e). The FWHM of GaSb QDs peaks varied in the range of 145 - 180 meV at both temperatures. It is reduced by increasing laser excitation power while the FWHM of GaAs steadily increases as a function of laser power. At higher excitation powers (256-340 mW), the FWHM of GaSb QDs is nearly constant (148 meV) for the temperature 20 K. When the temperature is increased to 30 K, the FWHM of QDs peaks (176-320 mW) slightly decreases from 159.8 meV to 149 meV. In comparison with the FWHM of GaAs at 20 K, that of GaAs at 30 K is getting high quickly till 146 meV which is nearly the same as GaSb QDs at excitation power of 320 mW. These values are larger than our previous report (104 meV).<sup>[7]</sup> We attribute it to large fluctuation of QD size (see Fig. 3) as well as high material intermixing. The latter can be modelled by considering  $\text{GaAs}_x\text{Sb}_{1-x}$  QDs with the As content  $x$  in QDs.<sup>[20]</sup> The high degree of As-Sb intermixing

in the range of 55-85% is due to the Sb/As exchange reaction during growth and capping.

## 4. CONCLUSIONS

In this work, we have investigated both structural and optical properties of GaSb/GaAs QDs grown on (001) Ge substrates. Due to the polar/non-polar effect of GaAs growth on Ge, the APD and APB are formed. Array of GaSb/GaAs QDs with an areal density of  $\sim 1.66 \times 10^{10} \text{ cm}^{-2}$  is obtained. QDs are observed on both APB and non-APB surfaces. This observation reveals that the APB does not affect to the formation of QDs. The strain by the QD layer is investigated by Raman spectroscopy. Optical properties are characterized by power-dependent PL measurement at 20 K and 30 K. PL from GaSb QDs is observed. In spite of redshift PL peaks at 20 K, type II band alignment feature of blueshift PL peaks is observed at 30 K. It shows some variations of peak position, integrated peak intensity and FWHM. The observed peak positions and spectral broadening are explained by QD size distribution as well as material intermixing in Ga(As)Sb/GaAs QDs. Optical properties of GaSb QDs are reported. The improving of optical properties such as tuning of photo response of QDs to longer wavelength by reducing the Sb/As intermixing at the interfaces and investigating the electrical properties of type II GaSb/GaAs QDs on Ge with APD are subjects of our future works.

## ACKNOWLEDGEMENTS

This research was financially supported by the Research Chair Grant, the National Science and Technology Development Agency (NSTDA), Thailand, Asian Office of Aerospace Research and Development (AOARD), Office of Naval Research Global (ONRG), Thailand Research Fund (TRF), National Nanotechnology Center (NANOTEC), ASEAN University Network/Southeast Asia Engineering Education Development Network (AUN/SEED-Net) and Chulalongkorn University.

## REFERENCES

- Y. Okada, N. J. Ekins-Daukes, T. Kita, R. Tamaki, M. Yoshida, A. Pusch, O. Hess, C. C. Philips, D. J. Farrell, K. Yoshida, N. Ahsan, Y. Shoji, T. Sogabe, and J.-F. Guillemoles, *Appl. Phys. Rev.* **2**, 0021302 (2015).
- K. Laouthaiwattana, O. Tangmattajittakul, S. Suraprapapich, S. Thainoi, P. Changmuang, S. Kanjanachuchai, S. Ratanathamphan, and S. Panyakeow, *Sol. Energ. Mat. Sol. C.* **93**, 746 (2009).
- S. Kiravittaya, U. Manmontri, S. Sopitpan, S. Ratanathamphan, C. Antarasen, M. Sawadsaringkarn, and S. Panyakeow, *Sol. Energ. Mat. Sol. C.* **68**, 89 (2001).
- P. J. Carrington, A. S. Mahajumi, M. C. Wagener, J. R. Botha, Q. Zhuang, and A. Krier, *Physica B* **407**, 1493 (2012).
- F. Xu, X.-G. Yang, S. Luo, Z.-R. Lv, and T. Yang, *J. Appl. Phys.* **116**, 133102 (2014).
- W. Tantiweerasophon, S. Thainoi, P. Changmuang, S. Kanjanachuchai, S. Ratanathamphan, and S. Panyakeow, *J. Cryst. Growth* **323**, 254 (2010).
- M. Kunrugsa, S. Kiravittaya, S. Sopitpan, S. Ratanathamphan, and S. Panyakeow, *J. Cryst. Growth* **401**, 441 (2014).
- M. Bosi and G. Attolini, *Prog. Cryst. Growth Ch.* **56**, 146 (2010).
- L. Lazzarini, L. Nazi, G. Salviati, C. Z. Fregonara, Y. Li, L. J. Gilling, C. Hardingham, and D. B. Holt, *Micron* **31**, 217 (2000).
- M. Hayne, R. J. Young, E. P. Smakman, T. Nowozin, P. Hodgson, J. K. Garleff, P. Rambabu, P. M. Koenraad, A. Marent, L. Bonato, A. Schliwa, and D. Bimberg, *J. Phys. D* **46**, 264001 (2013).
- K. Yamaguchi, S. Tsukamoto, and K. Matsuda, *Handbook of Self Assembled Semiconductor Nanostructure for Novel Devices in Photonics and Electronics* (Chapter 8), p. 271, Z. Wang (Ed.) (2008).
- J. Oh and J. C. Campbell, *Mater. Sci. Semicond. Process.* **13**, 185 (2010).
- K. Reginski, J. Muszalski, V. V. Preobrazhenskii, and D. I. Lubyshev, *Thin Solid Films* **267**, 54 (1995).
- E. P. Smakman, J. K. Garleff, R. J. Young, M. Hayne, P. Rambabu, and P. M. Koenraad, *Appl. Phys. Lett.* **100**, 142116 (2012).
- D. Kohen, S. Bao, K. H. Lee, K. E. K. Lee, C. S. Tan, S. F. Yoon, and E. A. Fitzgerald, *J. Cryst. Growth* **421**, 58 (2015).
- A. Ito, M. Ichimura, A. Usami, T. Wada, and H. Kano, *J. Appl. Phys.* **72**, 2531 (1992).
- K. Suzuki and Y. Arakawa, *J. Cryst. Growth* **201/202**, 1205 (1999).
- C. Jiang and H. Sakaki, *Physica E* **26**, 180 (2005).
- F. Hatami, M. Grundmann, N. N. Ledentsov, F. Heinrichsdorff, R. Heitz, J. Böhrer, D. Bimberg, S. S. Ruvimov, P. Werner, V. M. Ustinov, P. S. Kop'ev, and Z. I. Alferov, *Phys. Rev. B* **57**, 4635 (1998).
- S. Kiravittaya, Zon, T. Poempool, S. Thainoi, S. Kanjanachuchai, S. Ratanathamphan, and S. Panyakeow, *ECTICON* (2016). (accepted)